JEM Journal of Experimental Medicine

BRIEF DEFINITIVE REPORT

A defect in COPI-mediated transport of STING causes immune dysregulation in COPA syndrome

Zimu Deng[1*], Zhenlu Chong[1*], Christopher S. Law[1], Kojiro Mukai[2], Frances O. Ho[1], Tereza Martinu[3], Bradley J. Backes[1], Walter L. Eckalbar[1], Tomohiko Taguchi[2], and Anthony K. Shum[1,4]

Pathogenic *COPA* variants cause a Mendelian syndrome of immune dysregulation with elevated type I interferon signaling. COPA is a subunit of coat protein complex I (COPI) that mediates Golgi to ER transport. Missense mutations of the COPA WD40 domain impair binding and sorting of proteins targeted for ER retrieval, but how this causes disease remains unknown. Given the importance of COPA in Golgi–ER transport, we speculated that type I interferon signaling in COPA syndrome involves missorting of STING. We show that a defect in COPI transport causes ligand-independent activation of STING. Furthermore, SURF4 is an adapter molecule that facilitates COPA-mediated retrieval of STING at the Golgi. Activated STING stimulates type I interferon–driven inflammation in *Copa*$^{E241K/+}$ mice that is rescued in STING-deficient animals. Our results demonstrate that COPA maintains immune homeostasis by regulating STING transport at the Golgi. In addition, activated STING contributes to immune dysregulation in COPA syndrome and may be a new molecular target in treating the disease.

Introduction

COPA syndrome is a genetic disorder of immune dysregulation caused by missense mutations that disrupt the WD40 domain of coatomer protein complex subunit a (COPA; Watkin et al., 2015). COPA is a subunit of coat protein complex I (COPI) that mediates retrograde movement of proteins from the Golgi apparatus to the ER (Adolf et al., 2019). Prior studies have shown that alterations to the COPA WD40 domain lead to impaired binding and sorting of proteins bearing a C-terminal dilysine motif as well as a defect in retrograde Golgi to ER transport (Eugster et al., 2000; Watkin et al., 2015). To date, the molecular mechanisms of COPA syndrome remain unknown, including whether missorted proteins are critical for initiating the disease.

A clue to the pathogenesis of COPA syndrome recently arose with the observation that type I interferon signaling appears to be highly dysregulated in the disease (Volpi et al., 2018). This led us to investigate whether COPA syndrome shares features with any of the well-described Mendelian interferonopathy disorders (Uggenti et al., 2019). COPA syndrome manifests similarly to the type I interferonopathy STING-associated vasculopathy with onset in infancy (SAVI). Both diseases present at an early age with interstitial lung disease, activation of type I interferon–stimulated genes (ISGs), and evidence of capillaritis (Tsui et al., 2018; Liu et al., 2014).

Stimulator of interferon genes (STING) is an ER-localized transmembrane protein involved in innate immune responses to cytosolic nucleic acids. After binding cyclic dinucleotides, STING becomes activated as it translocates to the ER-Golgi intermediate compartment and Golgi. At the ER-Golgi intermediate compartment/Golgi, STING forms multimers and activates the kinase TBK1 which subsequently phosphorylates the transcription factor IRF3 to induce expression of type I interferons and other cytokines (Gui et al., 2019). In SAVI, gain-of-function mutations cause STING to aberrantly exit the ER and traffic to the Golgi and become activated (Dobbs et al., 2015). Prior work has suggested that COPI may be involved in STING transport at the Golgi, but this is not well established, and the molecular interactions between COPI and STING remain unknown (Gui et al., 2019; Ablasser and Hur, 2020). Because COPA plays a critical role in mediating Golgi to ER transport, we hypothesized that activation of type I interferon signaling in COPA syndrome involves missorting of STING.

Results and discussion

To examine this, we assessed lung fibroblasts from a COPA syndrome patient to determine if there was evidence of STING

[1]Department of Medicine, University of California, San Francisco, San Francisco, CA; [2]Laboratory of Organelle Pathophysiology, Department of Integrative Life Sciences, Graduate School of Life Sciences, Tohoku University, Sendai, Japan; [3]Toronto Lung Transplant Program, University Health Network, University of Toronto, Toronto, Ontario, Canada; [4]Cardiovascular Research Institute, University of California, San Francisco, San Francisco, CA.

*Z. Deng and Z. Chong contributed equally to this paper; Correspondence to Anthony K. Shum: anthony.shum@ucsf.edu.

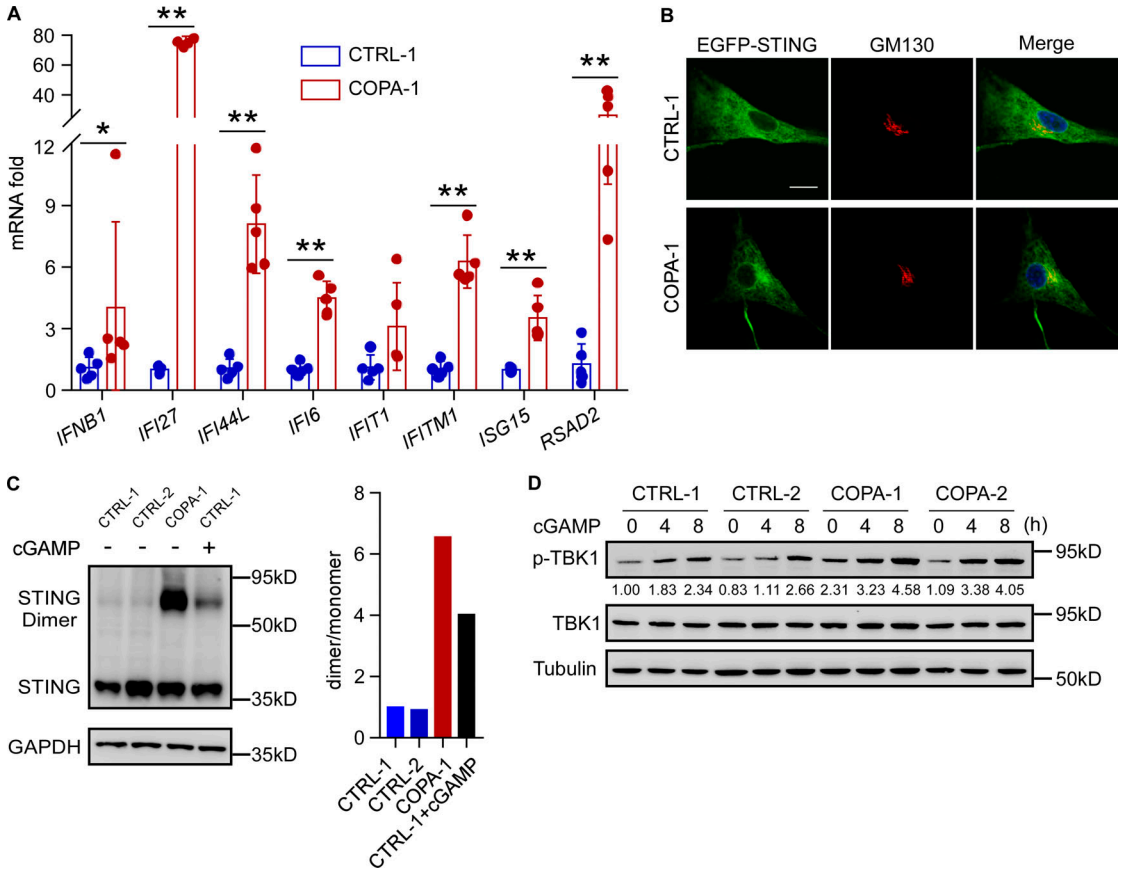

Figure 1. **COPA syndrome patient fibroblasts demonstrate spontaneous STING activation. (A)** Real-time PCR was performed for ISG expression in primary lung fibroblasts from a healthy control and a COPA syndrome subject. **(B)** Primary lung fibroblasts from a healthy control and a COPA syndrome subject were reconstituted with wild-type EFGP-STING retrovirus. The reconstituted cells were stained with indicated antibody, and localization of STING was observed using a confocal microscope. GM130 is a Golgi marker. **(C)** Immunoblots of endogenous STING in primary lung fibroblasts from two healthy controls and a COPA syndrome subject under nonreducing SDS-PAGE conditions with and without cGAMP (0.5 µg/ml) stimulation. **(D)** Immunoblots of indicated antibodies in primary lung fibroblasts with cGAMP (2 µg/ml) stimulation for indicated time (n = 2 per group). Data in A from five samples in two independent experiments represent means ± SD. *P < 0.05, **P < 0.01 (two-tailed Mann-Whitney U test). Scale bar, 20 µm in B.

activation. We measured mRNA transcript levels of several ISGs and found they were significantly elevated in comparison to healthy control lung fibroblasts in the presence or absence of a STING agonist (Fig. 1 A and Fig. S1, A and B). Confocal microscopy of COPA syndrome fibroblasts revealed prominent colocalization of STING with the Golgi (Fig. 1 B). Western blots of cellular protein lysates showed an increase in STING multimerization (Fig. 1 C) consistent with localization of STING at the Golgi and also higher levels of phosphorylated TBK1 (pTBK1) and phosphorylated STING (Fig. 1 D and Fig. S1 C), indicative of STING activation (Srikanth et al., 2019). These data suggest that the elevated type I ISGs observed in COPA syndrome patients may be caused by spontaneous activation of STING.

To establish the specific role of mutant COPA in triggering STING pathway activation, we transduced cells with retroviral vectors encoding enhanced GFP (EGFP)–STING and then transfected them with plasmids encoding wild-type or E241K mutant COPA. We performed confocal microscopy to examine whether mutant COPA caused STING to localize on the Golgi, similar to what we observed in patient fibroblasts. In cells expressing wild-type COPA, EGFP-STING was normally distributed throughout the cytoplasm (Gui et al., 2019), whereas in cells with E241K mutant COPA, EGFP-STING colocalized with the Golgi marker GM130 (Fig. 2 A). We next reconstituted human embryonic kidney 293 cell line (HEK293)T cells (which lack endogenous STING) with retroviral vectors encoding EGFP-STING and then transfected cells with wild-type or E241K mutant COPA. We found that even in the absence of a STING agonist, cells demonstrated a significant increase in pTBK1 (Fig. 2 B) and higher levels of mRNA transcripts encoding *IFNB1* and type I ISGs (Fig. 2 C). Importantly, all of these increases were abolished in HEK293T cells without EGFP-STING, indicating that mutant COPA activates TBK1 and type I interferon signaling specifically through STING rather than other innate immune pathways such as TIR-domain–containing adapter-inducing interferon β or mitochondrial antiviral signaling protein (Fig. 2, B and C; Liu et al., 2015). Taken together, these data show that mutant COPA causes ligand-independent activation of STING on the Golgi with up-regulation of type I interferon signaling.

We hypothesized that retention of STING on the Golgi might reflect a failure of STING to be taken up into mutant COPA containing COPI complexes for transport to the ER. To evaluate

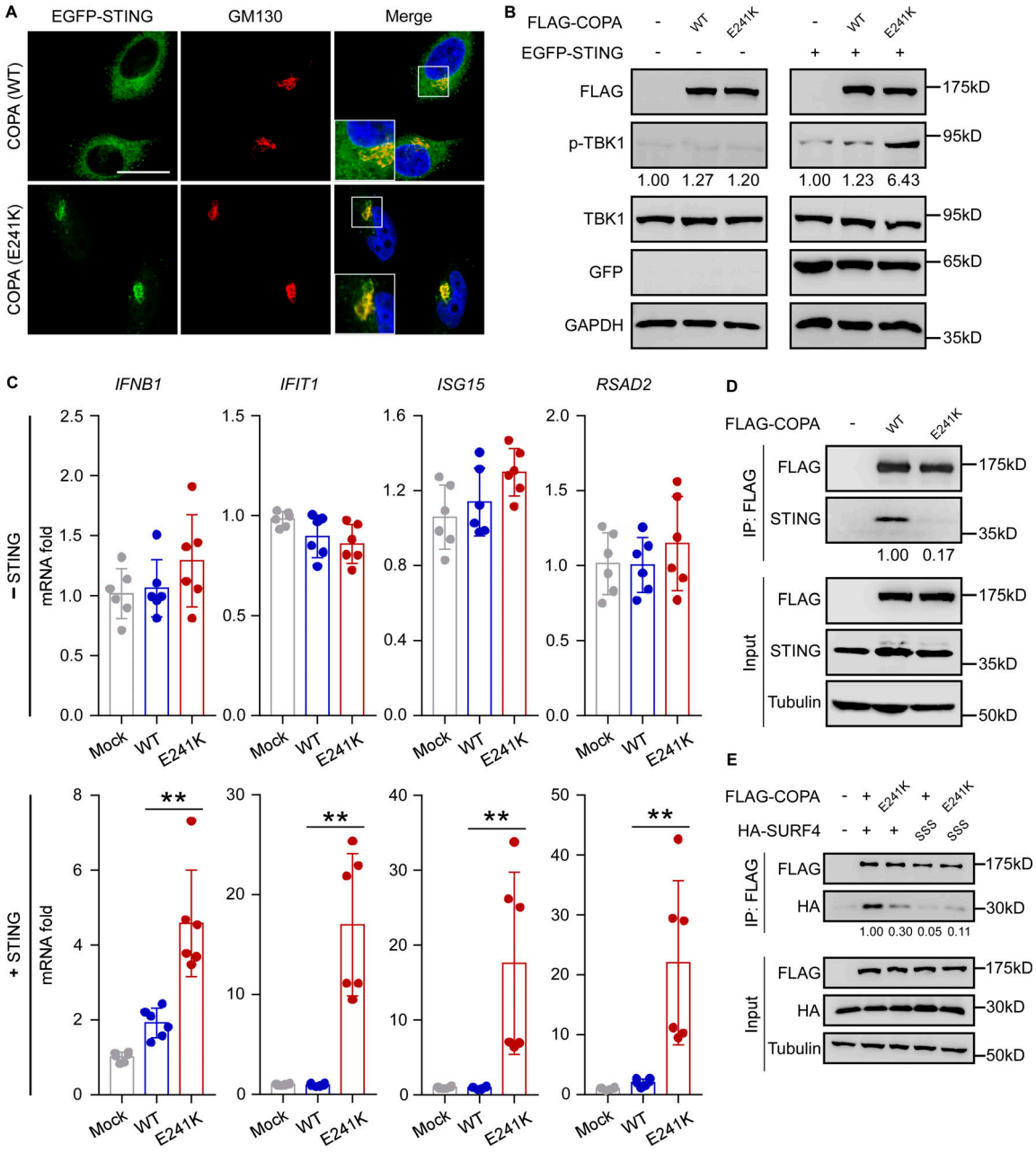

Figure 2. **Activated STING is retained on the Golgi after failed retrieval of SURF4 by mutant COPA. (A)** HeLa cells reconstituted with WT EGFP-STING retrovirus and transfected with WT COPA or mutant COPA (E241K) for 24 h. Cells were stained with indicated antibodies, and localization of STING was observed using a confocal microscope. GM130 is a Golgi marker. Insets show enlarged field of EGFP-STING and GM130 colocalization. **(B)** HEK293T cells with and without EGFP-STING were transfected with WT or mutant COPA (E241K) for 24 h, and then immunoblot was performed with indicated antibodies. **(C)** HEK293T cells with and without EGFP-STING were transfected with WT or mutant COPA (E241K) for 24 h, and then real-time PCR was performed for ISG expression. **(D)** FLAG IPs from lysates of HEK293 cells overexpressing FLAG-tagged COPA (WT/E241K) were immunoblotted for indicated antibodies. **(E)** FLAG IPs from lysates of HEK293T cells overexpressing FLAG-tagged COPA (WT/E241K) and HA-tagged SURF4 (WT/SSS-mutant) immunoblotted for indicated antibodies. Data in C from six samples in two independent experiments represent means ± SD. **P < 0.01 (two-tailed Mann-Whitney *U* test). Scale bar, 20 µm in A.

this, we analyzed the protein–protein interaction between COPA and STING. We performed coimmunoprecipitation experiments and found that although we could pull down STING with wild-type COPA, the amount of STING that coimmunoprecipitated with E241K mutant COPA was substantially reduced (Fig. 2 D). We previously showed that disease-causative *COPA* mutations cause a defect in binding between the COPA WD40 domain and C-terminal dilysine motif (e.g., KKxx and KxKxx) of proteins targeted for retrieval to the ER (Watkin et al., 2015). Because STING lacks a dilysine tag, we hypothesized that an adaptor protein mediates the interaction between STING and COPA. A review of published studies uncovered seven STING interacting partners that contain a C-terminal dilysine motif (Fig. S2 A; Lee et al., 2013; Huttlin et al., 2017; Shang et al., 2018; Li et al., 2011).

Among these, surfeit 4 (SURF4) was the only protein shown to cycle between the ER and the Golgi via COPI (Mitrovic et al., 2008; Adolf et al., 2019) and function as a cargo receptor (Emmer et al., 2018). Thus, we speculated that SURF4 was a likely candidate for mediating an interaction between COPA and STING. We confirmed through coimmunoprecipitation assays that SURF4 associates with STING and COPA (Fig. 2 E and Fig. S2 B) and then mutated the C-terminal dilysine motif of SURF4 by replacing the lysines at positions -3, -4, and -5 from the C terminus with serines (SURF4-SSS). The amount of SURF4-SSS pulled down with COPA was significantly less than with wild-type SURF4, demonstrating the importance of the dilysine motif to the SURF4–COPA interaction (Fig. 2 E). Consistent with this, we found that the association between SURF4 and mutant COPA was markedly reduced in comparison to wild-type COPA, reflecting a defect in binding between the mutant COPA WD40 domain and SURF4 dilysine tag (Fig. 2 E). Finally, as further evidence that SURF4 functions as an adapter molecule for STING and COPA, loss of SURF4 led to a reduction in the amount of STING that coimmunoprecipitated with wild-type COPA (Fig. S2 C) and also led to an increase in transcript levels of *Ifnb1* and type I ISGs (Fig. S2 D). In aggregate, our data suggest that SURF4 functions as a cargo receptor for STING and that mutant COPA is unable to bind SURF4 and incorporate STING into COPI vesicles. This results in retention of STING on the Golgi, where it becomes spontaneously activated and triggers type I interferon signaling.

We next turned to a mouse model of COPA syndrome to understand how mutant COPA-mediated STING activation causes immune dysregulation in vivo. We previously reported that *Copa*$^{E241K/+}$ mice, which express one of the same disease-causative mutations as patients, spontaneously develop activated cytokine-secreting T cells and T cell–mediated lung disease (Deng et al., 2020). Through bone marrow chimera and thymic transplant experiments, we showed that mutant COPA within thymic epithelial cells perturbs thymocyte development and leads to a defect in immune tolerance. Because STING is highly expressed in thymic tissue (Manils et al., 2017), we wondered how missorting of STING due to mutant COPA might contribute to the T cell phenotypes we observed in *Copa*$^{E241K/+}$ mice.

To evaluate this, we first confirmed that *Copa*$^{E241K/+}$ mice demonstrate retention of activated STING on the Golgi with elevated type I interferon signaling, similar to what we observed in patient cells and our transfection assays (Fig. 3, A–C). We next performed bulk RNA sequencing to identify gene expression programs that were altered in thymic epithelial cells. Among the differentially expressed genes, we found significant up-regulation of *Ifnb* and several type I ISGs, consistent with STING activation (Fig. 4 A). Thymocytes migrating through the thymic epithelium were impacted by higher *Ifnb* levels because they exhibited an elevated type I interferon signature (Fig. 4 B) and higher levels of Qa2 (Fig. 4 C), a cell surface marker expressed in response to IFN-β. We examined thymocyte populations using a staining protocol that subsets increasingly mature single positive (SP) cells into semi-mature (SM), mature 1 (M1), and mature 2 (M2) populations (Fig. 4 D). Prior studies found that type I interferons are required during the transition of thymocytes

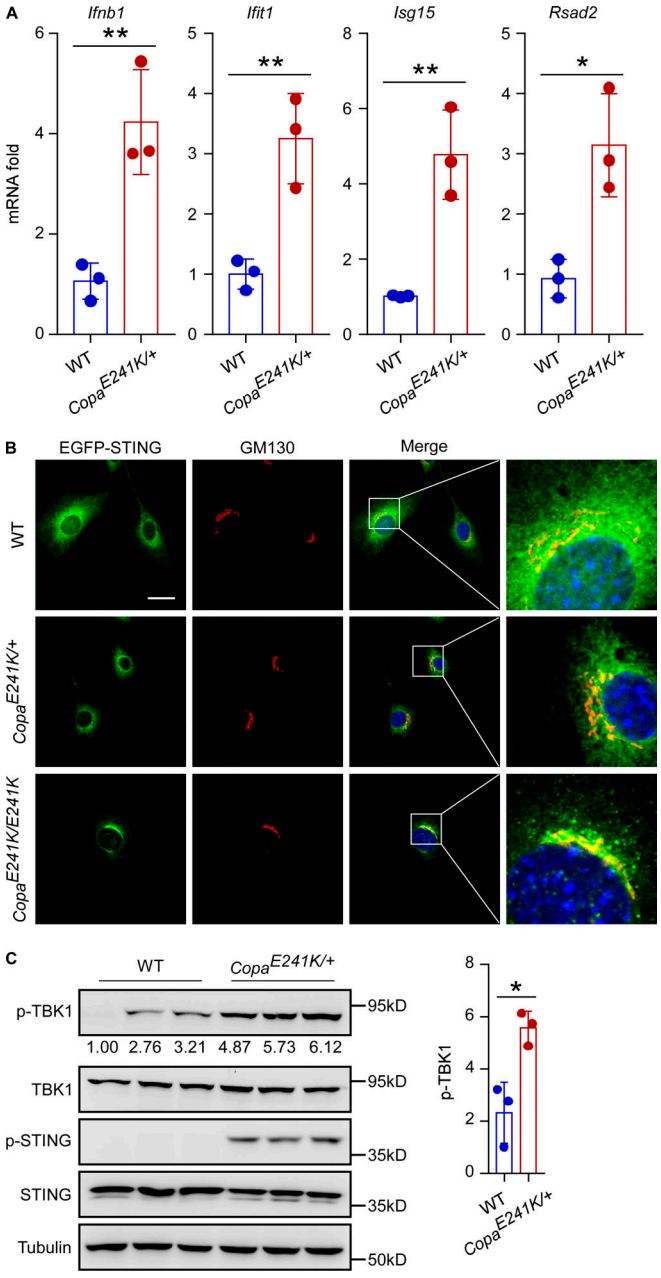

Figure 3. ***Copa*$^{E241K/+}$ mice exhibit STING activation with elevated type I interferon signaling. (A)** Real-time PCR was performed for ISG expression in immortalized MEF cells derived from three WT and three *Copa*$^{E241K/+}$ mice. **(B)** Immortalized MEF cells from WT, *Copa*$^{E241K/+}$, and *Copa*$^{E241K/E241K}$ mice were reconstituted with WT EGFP-STING retrovirus. The reconstituted cells were stained with the indicated antibodies, and localization of STING was observed using a confocal microscope. GM130 is a Golgi marker. Insets show enlarged field of EGFP-STING and GM130 colocalization. **(C)** Immunoblot was performed with the indicated antibodies in splenocytes from WT or *Copa*$^{E241K/+}$ mice (n = 3 for each genotype). Data in A and C are means ± SD. *P < 0.05, **P < 0.01 (unpaired two-tailed Student's t tests). Scale bar, 20 µm in B.

from SM to M2 cells (Xing et al., 2016). In *Copa*$^{E241K/+}$ mice, we found a significant increase in the proportion of M2 cells (Fig. 4 D), suggesting that higher IFN-β levels promoted an expansion of late-stage thymocytes.

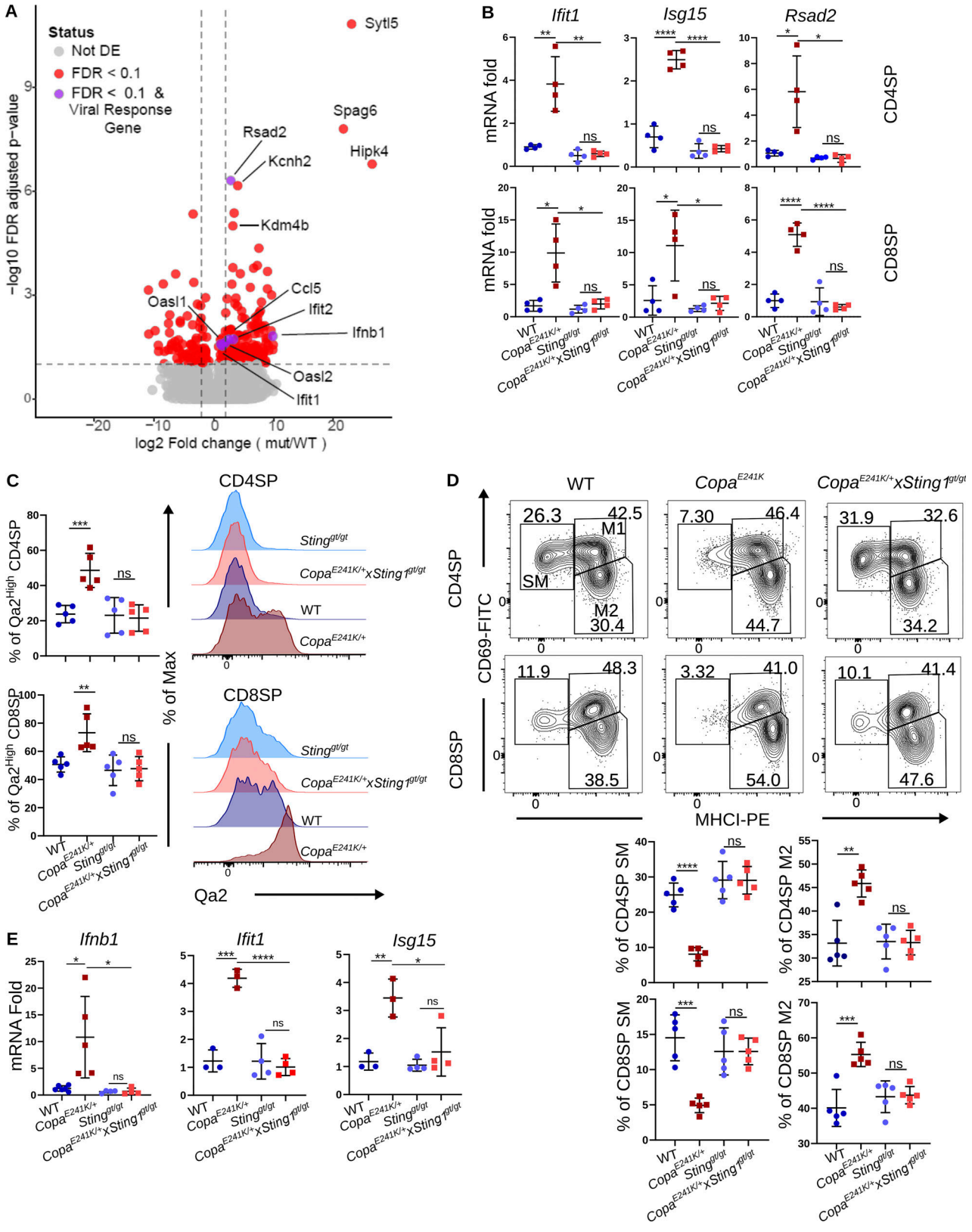

Figure 4. **Activated STING perturbs thymocyte development by increasing type I interferons in the thymus. (A)** Medullary thymic epithelial cells sorted from WT and *Copa*$^{E241K/+}$ mice were used for RNA-sequencing analysis (n = 3 each genotype). Volcano plot of the differentially affected genes (FDR < 0.1, red; FDR < 0.1, ISG from viral response Gene Ontology categories, purple). **(B)** Real-time PCR performed for *Ifit1*, *Rsad2*, and *Isg15* expression in SP thymocytes (top: CD4SP; bottom: CD8SP). n = 4 mice each genotype, two independent experiments. **(C)** Left: Percentages of Qa2^{high} population among SP thymocytes (top: CD4SP; bottom: CD8SP). Right: Representative flow analysis of Qa2 expression on SP thymocytes (top: CD4SP; bottom: CD8SP). n = 5 each genotype, three independent experiments. **(D)** Top: CD69 versus MHCI expression on SP thymocytes (top: CD4SP; bottom: CD8SP). Bottom: Percentages of SM and M2

populations among SP thymocytes (top: CD4SP; bottom: CD8SP). n = 5 each genotype, three independent experiments. **(E)** Real-time PCR performed for *Ifnb1*, *Ifit1*, and *Isg15* expression in thymic epithelial cells (CD45$^-$, Epcam$^+$, Ly51$^-$, MHC-II^{high} medullary thymic epithelial cell). $n \geq 3$ each genotype, two independent experiments. Data in B–F represent means ± SD. *P < 0.05, **P < 0.01, ***P < 0.001, ****P < 0.0001; ns, not significant (unpaired, parametric, two-tailed Student's t test).

To determine the role of STING in these changes, we crossed *Copa*$^{E241K/+}$ mice to STING-deficient *Sting1*$^{gt/gt}$ mice. We measured mRNA transcripts of thymic epithelial cells for *Ifnb1* and type I ISGs and found that all of the increases returned to wild-type levels in *Copa*$^{E241K/+}$×*Sting1*$^{gt/gt}$ mice (Fig. 4 E). In addition, loss of STING abrogated all of the thymocyte phenotypes caused by mutant COPA, including the elevated type I interferon signature, increased Qa2 expression, and higher proportion of M2 cells (Fig. 4, C–E). Taken together, these data indicate that activated STING in the thymus of *Copa*$^{E241K/+}$ mice perturbs T cell development by elevating type I interferons to promote late-stage thymocyte maturation.

We next focused on peripheral lymphoid organs to examine whether mutant COPA-mediated STING activation contributed to systemic inflammation in *Copa*$^{E241K/+}$ mice. We reasoned that if STING were to have a significant role in systemic disease, this would provide an opportunity to test whether targeting STING activation dampens systemic inflammation in COPA syndrome patients. Splenocytes from *Copa*$^{E241K/+}$ mice had a significant increase in type I ISGs that completely reverted to wild-type levels in *Copa*$^{E241K/+}$×*Sting1*$^{gt/gt}$ mice (Fig. S3 A). An analysis of peripheral T cell populations revealed that STING deficiency reversed the significant increase in activated effector memory cells and cytokine-secreting T cells caused by mutant COPA (Fig. 5 A and Fig. S3, B–D). Finally, in strong support of STING being a critical mediator of disease in COPA syndrome pathogenesis, we found that loss of STING rescued embryonic lethality of homozygous *Copa*$^{E241K/E241K}$ mice. We recovered no *Copa*$^{E241K/E241K}$ pups in over five litters from our *Copa*$^{E241K/+}$ × *Copa*$^{E241K/+}$ breeding, although 17 *Copa*$^{E241K/E241K}$ mice were born out of 40 pups in five litters from *Copa*$^{E241K/+}$×*Sting1*$^{gt/gt}$ parents. In aggregate, these data indicate that STING contributes to immune dysregulation in *Copa*$^{E241K/+}$ mice and that targeting STING in COPA syndrome may be an important therapy for patients.

Activation of STING requires palmitoylation at the Golgi (Mukai et al., 2016), and recent studies report that inhibition of activation-induced palmitoylation of STING with small molecules prevents multimerization of the protein and recruitment of downstream signaling partners (Haag et al., 2018). We treated splenocytes from *Copa*$^{E241K/+}$ mice with C-176 mouse STING inhibitor and found that this was highly effective at dampening activation of type I ISGs (Fig. 5 B). We then took peripheral blood mononuclear cells (PBMCs) from a COPA syndrome patient or healthy control subject and treated them with the small-molecule human STING inhibitor H-151. In parallel, we treated PBMCs with a JAK-STAT inhibitor, since drugs in this class have recently been reported as a clinical therapy for COPA syndrome (Krutzke et al., 2019). Although both the JAK-STAT inhibitor and STING inhibitor reduced type I ISGs, only the STING inhibitor was able to cause a decrease in the levels of the upstream cytokine IFN-β (Fig. 5, C and D). Our results suggest that targeting STING activation with small-molecule inhibitors might be an effective treatment for COPA syndrome patients with increased efficacy over current therapies.

This work establishes COPA as a critical regulator of STING transport that maintains immune homeostasis by mediating retrieval of STING from the Golgi. Defects in COPA function cause STING to multimerize and become spontaneously activated at the Golgi even in the absence of STING ligand, suggesting that at steady state, low levels of STING continuously cycle between the ER and Golgi. In support of our findings, Mukai et al. used cultured cells to show that retrograde transport by COPI is essential for maintaining STING in its dormant state, independent of cyclic guanosine monophosphate–adenosine monophosphate (cGAMP) synthase (Mukai et al., 2020 *Preprint*). Although we used a candidate approach to identify SURF4 as a putative cargo receptor that engages STING for incorporation into COPI vesicles by COPA, Mukai et al. directly tested 18 STING-binding proteins containing C-terminal dilysine motifs and found that knockdown of SURF4 was the only one that caused STING to localize on the Golgi. Future studies should address in greater depth whether SURF4 is a central mediator in STING transport and if other adapter molecules are involved. Taken together, our data suggest a role for SURF4 in mediating the retrieval of STING from the Golgi by COPI and provide new insight into the steady-state dynamics of STING transport in resting cells.

Missense mutations in *COPA* that lie in the WD40 domain impair retrograde transport of a broad range of COPI cargo proteins containing C-terminal dilysine motifs (Watkin et al., 2015). Despite this, our data suggest that impaired trafficking of STING in particular is key to the pathogenesis of COPA syndrome, since not only does loss of STING reverse many of the immunological derangements in our mouse model, but it also strikingly rescues embryonic lethality of homozygous mutant mice. Further study should be undertaken to determine whether other COPA cargo contributes to COPA syndrome pathogenesis independent of STING.

The ubiquitous expression of COPA has made it difficult to identify the cell types that are responsible for causing disease, particularly since COPA is not enriched in any specific immune or lung cell. The tissue specificity of STING may provide additional insight into the understanding of COPA syndrome and the organs most affected. One unexpected outcome of our work was the finding that STING has a functional role in thymic stromal tissue. Although thymic epithelial cells are known to be a significant source of type I interferons (Otero et al., 2013; Xing et al., 2016), the mechanisms regulating interferon secretion in the thymus remain largely unexplored. Interestingly, STING also modulates autophagy (Gui et al., 2019), which in thymic epithelial cells is essential for processing self-antigen peptides for presentation to thymocytes (Nedjic et al., 2008). Additional

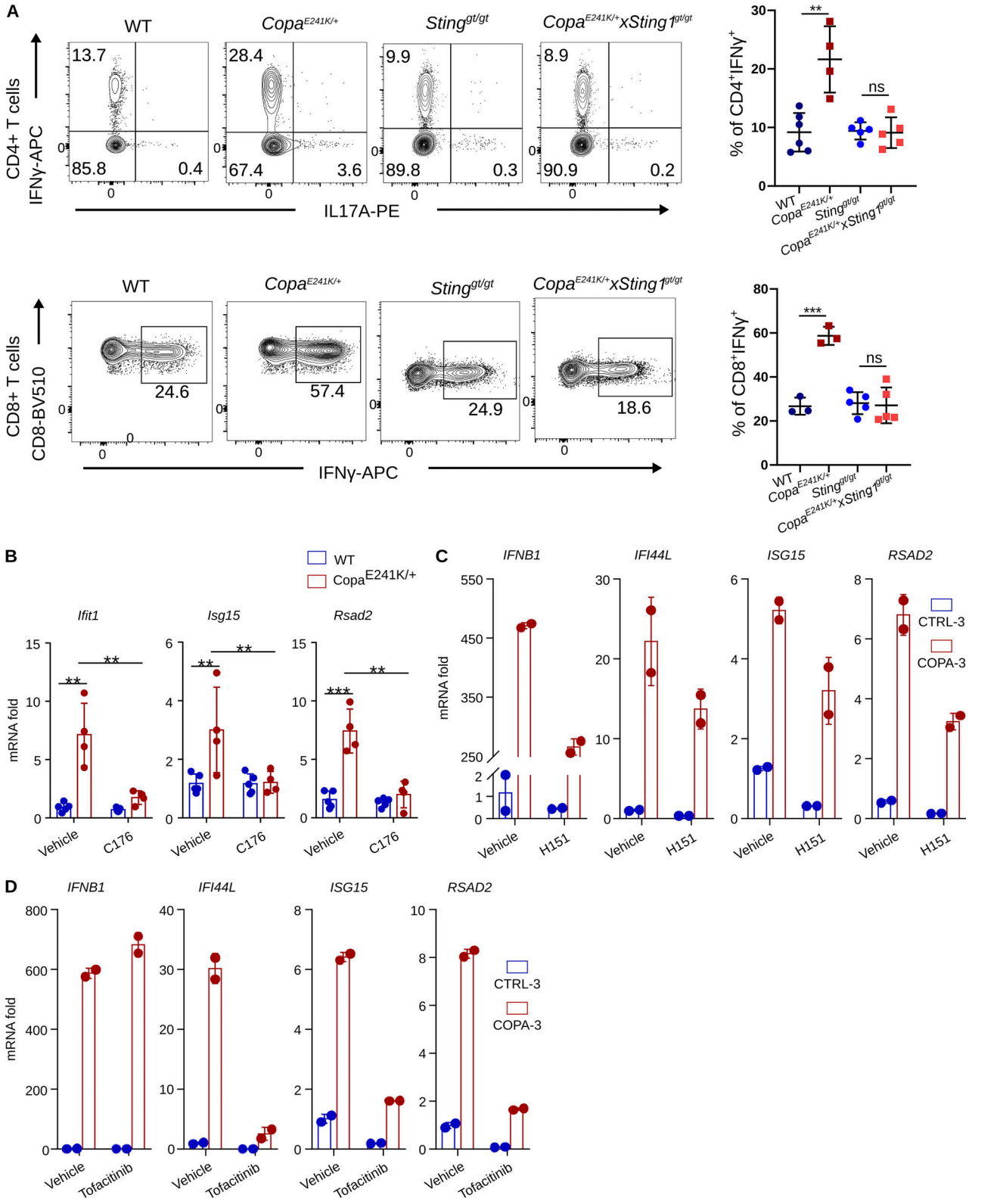

Figure 5. **Loss of STING function dampens inflammation caused by mutant COPA. (A)** Top left: Intracellular levels of IFN-γ and IL17A in splenic CD4+ T cells after PMA/ionomycin stimulation. Top right: Percentages of IFN-γ–producing CD4+ T cells. *n* ≥ 3 each genotype, more than three independent experiments. Bottom left: Intracellular IFN-γ production in splenic CD8+ T cells after PMA/ionomycin stimulation. Bottom right: percentages of IFN-γ–producing CD8+ T cells. *n* ≥ 3 each genotype, more than three independent experiments. **(B)** Real-time PCR for ISG expression in splenocytes harvested from four WT mice and four *Copa*$^{E241K/+}$ mice treated with or without STING inhibitor C-176 (10 µM) for 24 h. **(C and D)** Real-time PCR performed in duplicate for ISG expression in PBMCs from a healthy control and a COPA syndrome subject treated with or without STING inhibitor H-151 (10 µM; C) or JAK inhibitor tofacitinib (2 µM; D) for 24 h. Data represent means ± SD. **P < 0.01, ***P < 0.001; ns, not significant (unpaired, parametric, two-tailed Student's *t* tests).

research might address whether activated STING alters autophagic function in thymic epithelial cells and, if so, whether this impacts T cell selection.

Our work indicates that COPA syndrome belongs to a category of diseases defined by STING activation (Uggenti et al., 2019). Going forward, clinicians may want to compare and contrast clinical features and treatment approaches in COPA syndrome and SAVI to establish optimal care of patients. Understanding the mechanisms by which STING causes interstitial lung disease has the potential to substantially improve outcomes in both disorders (Tsui et al., 2018; Liu et al., 2014). For those with COPA syndrome, the dramatic reversal of immune dysregulation that we observed in $Copa^{E241K/+} \times Sting1^{gt/gt}$ mice provides some hope that small-molecule STING inhibition can be an effective molecularly targeted approach for treating this highly morbid disease.

Materials and methods

Reagents

2′3′-cGAMP and CP-690550 (tofacitinib) were purchased from InvivoGen. STING inhibitors C-176 and H-151 were synthesized by SYNthesis med chem at ≥99% purity by HPLC.

Plasmids

Human STING and SURF4 were subcloned from HEK293T cDNA into pCMV6-AC (Origene) with a FLAG tag at the C terminus or an HA tag at the N terminus, respectively. Plasmids expressing FLAG-tagged wild-type and mutant E241K human COPA were previously generated (Watkin et al., 2015). Retroviral plasmids expressing EGFP-tagged human and mouse STING were kindly provided by Dr. Tomohiko Taguchi (Tohoku University, Sendai, Japan).

Study subjects

Subjects were selected on the basis of COPA syndrome diagnosis, with their written informed consent, and were studied via protocols approved by the Research Ethics Board of Toronto General Hospital and the Institutional Review Boards for the protection of human subjects of Cleveland Clinic or the University of California, San Francisco (UCSF).

Isolation of human lung fibroblasts

Control lung tissue was harvested from anonymous brain-dead donors from the Northern California Transplant Donor Network. Screening criteria for selection of healthy lungs for specimen collection were previously described (Lee et al., 2009). Mutant lung explants were from two COPA syndrome patients receiving lung transplants. Fibroblasts were isolated as described (Ramos et al., 2001). In brief, tissue was minced with scissors into 5-mm pieces and digested three times with 0.25% trypsin (GE Healthcare Life Sciences) for 10 min at 37°C. The resulting cell and tissue suspension was collected, neutralized with complete media (45% Ham's F12, 45% DMEM, and 10% FBS), pelleted, plated onto FBS-coated 60-mm dishes, and cultured in 5% CO_2 at 37°C. Fibroblasts were ready to passage and use 1 wk following isolation.

Isolation of MEFs

MEFs were isolated as described (Durkin et al., 2013). In brief, day 13.5 embryos were washed with PBS, minced with scissors into 1–2 mm pieces, and digested three times with 0.25% trypsin for 10 min at 37°C. The cell suspension was neutralized with complete media (DMEM and 10% FBS), pelleted, resuspended in complete media, and cultured in 5% CO_2 at 37°C.

To create immortal MEFs, Phoenix packaging cells (kindly gifted by Dr. Mark Anderson, UCSF, San Francisco, CA) were transfected with pBABE-neo largeTcDNA plasmid (a gift from Robert A. Weinberg, Whitehead Institute for Biomedical Research, Cambridge, MA; Addgene plasmid #1780; http://n2t.net/addgene:1780; RRID:Addgene_1780; Hahn et al., 2002), and viral supernatant was collected 2 d later. Early-passage MEFs were incubated in viral supernatant for 2 d, and then transformed cells were selected with G418 (Teknova).

siRNA knockdown

Predesigned siRNA oligomers (ON-TARGETplus SMARTPool) for *SURF4* and transfection control (siGENOME RISC-Free) were obtained from Dharmacon and resuspended in RNase-free water at 10 µM. siRNAs were transfected in Opti-Mem media (Life Technologies) for 48 h with Lipofectamine RNAiMAX (Life Technologies) according to manufacturer's protocol.

Immunoblotting and antibodies

Cells were lysed in Cold Spring Harbor NP-40 lysis buffer (150 mM NaCl, 50 mM Tris, pH 8.0, and 1.0% Nonidet-P40) supplemented with protease and phosphatase inhibitors (PMSF, NaF, Na_3VO_4, and Roche PhosSTOP) and then centrifuged at 12,000 *g* for 15 min at 4°C to get cellular lysate. Equal amounts of protein were loaded and size separated on an SDS–PAGE gel and wet transferred onto polyvinylidene fluoride membrane. The membrane was blocked in tris-buffered saline and Tween 20 (TBS-T) buffer with 5% milk for 1 h at room temperature, followed by overnight incubation with primary antibodies diluted in TBS-T with 5% BSA. Membrane was washed three times with TBS-T buffer for 10 min, incubated at room temperature with HRP-conjugated IgG secondary antibody (Jackson Immunoresearch), washed three times with TBS-T for 10 min followed once with TBS buffer for 10 min, and then developed with SuperSignal West Femto Chemiluminescent Substrate (Life Technologies).

Rabbit antibodies against TBK1 (D1B4), pTBK1 (Ser172, D52C2), STING (D2P2F), p-STING (Ser365, D8F4W), p-STING (Ser366, D7C3S), FLAG (D6W5B), HA (C29F4), and GFP (D5.1) were from Cell Signaling Technology. Rabbit antibody against SURF4 was from Novus. Mouse antibodies against GAPDH and β-Tubulin were from Santa Cruz Biotechnology. Mouse antibody against GM130 was from BD Biosciences.

Coimmunoprecipitation

HEK293 or HEK293T cells transfected with indicated plasmids were collected, washed once with PBS, lysed in NP-40 lysis buffer supplemented with protease and phosphatase inhibitors, and centrifuged at 12,000 *g* for 15 min at 4°C. The supernatant was mixed with FLAG-M2 beads (Sigma) and incubated

overnight at 4°C. 10% of lysate was saved as input. The following day, the beads were washed three times with immunoprecipitate (IP) washing buffer (10 mM Tris, pH 7.4, 1 mM EDTA, 150 mM NaCl, and 1% Triton X-100) for 10 min. 2× SDS loading buffer (100 mM Tris, pH 6.8, 4% SDS, 20% glycerol, 10% β-mercaptoethanol, and 0.1% bromophenol blue) was added into the IP complex and boiled at 95°C for 5 min. Samples were analyzed by immunoblot as described above.

Confocal microscopy

Cells were seeded onto glass coverslips and treated as indicated. Cells then were fixed with 4% paraformaldehyde, permeabilized with 0.1% Triton X-100, and blocked with 3% BSA. Slides were incubated with primary antibody overnight at 4°C, incubated with fluorescent-conjugated secondary antibody for 1 h at room temperature, and followed with DAPI incubation for 10 min at room temperature. Slides were then mounted with FluorSave Reagent (Millipore) and kept at 4°C in the dark. Images were captured with a Leica TCS SPE microscope, 63× objective, and oil immersion.

Mice strains

Copa^{E241K} knock-in mice were generated in our laboratory (Deng et al., 2020). C57BL/6J-*Sting1*^{gt}/J (*Sting*$^{gt/gt}$) mice were purchased from The Jackson Laboratory. All mice were maintained in the specific pathogen–free facility at UCSF, and all protocols were approved by UCSF's Institutional Animal Care and Use Committee.

Flow cytometry and antibodies

Single-cell suspensions of thymocytes and splenocytes were prepared by mechanically disrupting the thymus and spleen. Cells were filtered through 40-µm filters (Genesee Scientific) into 15-ml conical tubes and maintained in RPMI 1640 containing 5% FBS on ice. Splenocytes were further subjected to red blood cell lysis (Biolegend). For evaluation of surface receptors, cells were blocked with 10 µg/ml anti-CD16/32 for 15 min at room temperature and then stained with indicated antibodies in FACS buffer (PBS and 2% FBS) on ice for 40 min.

For intracellular cytokine detection, freshly isolated splenocytes were stimulated by PMA (Sigma) and ionomycin (Sigma) in the presence of brefeldin A (Biolegend) for 4 h. Cells were collected and stained with Ghost Dye Violet 450 (Tonbo Biosciences) followed by surface staining. Cells were then washed, fixed at room temperature for 15 min (PBS and 1% neutral buffered formalin), permeabilized, and stained with antibodies against cytokines on ice (PBS, 2% FBS, and 0.2% saponin). All samples were acquired on LSRFortessa or FACSVerse (BD Biosciences) and analyzed using FlowJo software V10.

Antibodies to the following were purchased from Biolegend: CD8 (53–6.7), IFN-γ (XMG1.2), and Epcam (G8.8); from eBioscience: IL17A (eBio17B7), IL13 (eBio13A), MHC-II (I-A; NIMR-4), Qa2 (69H1-9-9); and from Tonbo Biosciences: CD4 (GK1.5), MHC-II (I-A/I-E; mM5/114.15.2). The CD16/CD32 (2.4G2) antibody was obtained from UCSF's Monoclonal Antibody Core.

Thymic epithelial cell isolation

Thymic epithelial cells were isolated as described (Miller et al., 2018). Briefly, thymi from 4-wk-old mice were minced with razor blades into 1–2-mm^3 pieces. The tissue fragments were collected and enzymatically digested three times (DMEM, 2% FBS, 100 µg/ml DNase I, and 100 µg/ml Liberase). The single-cell suspensions from each digestion were pooled into 20 ml of magnetic-activated cell sorting buffer (PBS, 0.5% BSA, and 2 mM EDTA) on ice. Total cells were washed and centrifugated using a three-layer Percoll gradient with specific gravities of 1.115, 1.065, and 1.0. Thymic stromal cells were enriched and collected from the Percoll-light fraction, between the 1.065 and 1.0 layers. Thymic stromal cells were washed, stained, and sorted to isolate MHC-II^{high}CD80^{high} medullary thymic epithelial cells by FACS.

RNA isolation and quantitative real-time PCR analysis

RNA was isolated with the EZNA Total RNA kit (Omega Bio-tek) and was reverse transcribed to cDNA with SuperScript III reverse transcription and oligo d(T)$_{16}$ primers (Invitrogen). Quantitative real-time PCR was performed on Bio-Rad CFX thermal cyclers with TaqMan Gene Expression assays from Life Technologies (*GAPDH*, Hs02786624_g1; *IFNB1*, Hs01077958_s1; *IFI6*, Hs00242571_m1; *IFI27*, Hs01086373_g1; *IFI44L*, Hs00915292_m1; *ISG15*, Hs01921425_s1; *IFIT1*, Hs03027069_s1; *IFITM1*, Hs00705137_s1; *RSAD2*, Hs00369813_m1; *Gapdh*, Mm99999915_g1; *Ifnb1*, Mm00439552_s1; *Ifit1*, Mm00515153_m1; *Ifi44l*, Mm00518988_m1; *Isg15*, Mm01705338_s1; *Rsad2*, Mm00491265_m1; and *S1pr1*, Mm00514644).

RNA sequencing and data analysis

RNA-sequencing libraries were generated by first using the Nugen Ovation method (Tecan 7102-A01) to create cDNA from the isolated RNA, the sequencing library was then created from cDNA using the Nextera XT method (Illumina; FC-131-1096). All libraries were combined and sequenced on Illumina HiSeq4000 lanes, yielding ∼300 million single-end, 50-bp reads. Sequencing reads were then aligned to the mouse reference genome and the ensemble annotation build (GRCm38.78) using STAR (Dobin et al., 2013; v2.4.2a). Read counts per gene were used as input to DESeq2 (Love et al., 2014; v1.26.0) to test for differential gene expression between conditions using a Wald test. Genes passing a multiple-testing correct P value of 0.1 (false discovery rate [FDR] method) were considered significant. Pathway analysis was performed using DAVID (Huang et al., 2007) and the R/Bioconductor package RDAVIDWebService (Fresno and Fernández, 2013; v1.24.0).

Statistical analysis

All statistical analysis was performed using Prism 7 (GraphPad Software) or R 4.0.0 (R Foundation for Statistical Computing). Where indicated, two-tailed Mann-Whitney *U* test and unpaired, parametric, two-tailed Student's *t* test were used to evaluate the statistical significance between two groups, and $P < 0.05$ was considered statistically significant.

Data availability

The bulk RNA sequencing data are available at the Gene Expression Omnibus (GEO accession no. GSE153822).

Online supplemental material

Fig. S1 shows STING activation in lung fibroblasts isolated from a COPA syndrome patient. Fig. S2 is evidence of SURF4's role in

STING retrieval via COPA. Fig. S3 demonstrates type I interferon–driven inflammation in *Copa*$^{E241K/+}$ mice due to STING activation.

Acknowledgments

We thank Suzy A.A. Comhair and Serpil C. Erzurum from Cleveland Clinic Foundation for help providing lung explants; Paul Wolters, Tien Peng, Chaoqun Wang, and N. Soledad Reyes de Mochel at UCSF for help with providing lung explants; David J. Erle for discussions and assistance with RNA sequencing; and Mark S. Anderson for discussions and review.

This work was supported by the UCSF Program for Breakthrough Biomedical Research, funded in part by the Sandler Foundation (to A.K. Shum); National Institutes of Health (NIH)/National Institute of Allergy and Infectious Diseases (NIAID) R01AI137249 (to A.K. Shum), NIH/National Heart, Lung, and Blood Institute (NHLBI) R01HL122533 (to A.K. Shum), NIH/NHLBI R00HL135403 (to W.L. Eckalbar), and NIH/NHLBI PO1HL103453 (Suzy A.A. Comhair and Serpil C. Erzurum); Japan Society for the Promotion of Science KAKENHI grants JP19H00974 (to T. Taguchi), JP15H05903 (to T. Taguchi), JP17K15445 (to K. Mukai), and JP20H03202 (to K. Mukai); and AMED-PRIME (17939604 to T. Taguchi).

Author contributions: Z. Deng and Z. Chong designed and performed experiments and analyzed data. K. Mukai and T. Taguchi provided technical advice. C.S. Law performed experiments and analyzed data. F.O. Ho performed experiments. B.J. Backes assisted with small-molecule experimental design. W.L. Eckalbar analyzed RNA-sequencing data. T. Martinu provided lung explant tissue. A.K. Shum directed the study and wrote the manuscript.

Disclosures: T. Martinu reported grants from Sanofi and nonfinancial support from APCBio outside the submitted work. No other disclosures were reported.

Submitted: 21 May 2020
Revised: 7 July 2020
Accepted: 8 July 2020

References

Ablasser, A., and S. Hur. 2020. Regulation of cGAS- and RLR-mediated immunity to nucleic acids. *Nat. Immunol.* 21:17–29. https://doi.org/10.1038/s41590-019-0556-1

Adolf, F., M. Rhiel, B. Hessling, Q. Gao, A. Hellwig, J. Béthune, and F.T. Wieland. 2019. Proteomic Profiling of Mammalian COPII and COPI Vesicles. *Cell Rep.* 26:250–265.e5: E5. https://doi.org/10.1016/j.celrep.2018.12.041

Deng, Z., C.S. Law, F.O. Ho, K.M. Wang, K.D. Jones, J.-S. Shin, and A.K. Shum. 2020. A Defect in Thymic Tolerance Causes T Cell-Mediated Autoimmunity in a Murine Model of COPA Syndrome. *J. Immunol.* 204:2360–2373. https://doi.org/10.4049/jimmunol.2000028

Dobbs, N., N. Burnaevskiy, D. Chen, V.K. Gonugunta, N.M. Alto, and N. Yan. 2015. STING Activation by Translocation from the ER Is Associated with Infection and Autoinflammatory Disease. *Cell Host Microbe.* 18:157–168. https://doi.org/10.1016/j.chom.2015.07.001

Dobin, A., C.A. Davis, F. Schlesinger, J. Drenkow, C. Zaleski, S. Jha, P. Batut, M. Chaisson, and T.R. Gingeras. 2013. STAR: ultrafast universal RNA-seq aligner. *Bioinformatics.* 29:15–21. https://doi.org/10.1093/bioinformatics/bts635

Durkin, M.E., X. Qian, N.C. Popescu, and D.R. Lowy. 2013. Isolation of Mouse Embryo Fibroblasts. *Bio Protoc.* 3. e908. https://doi.org/10.21769/BioProtoc.908

Emmer, B.T., G.G. Hesketh, E. Kotnik, V.T. Tang, P.J. Lascuna, J. Xiang, A.-C. Gingras, X.-W. Chen, and D. Ginsburg. 2018. The cargo receptor SURF4 promotes the efficient cellular secretion of PCSK9. *eLife.* 7. e38839. https://doi.org/10.7554/eLife.38839

Eugster, A., G. Frigerio, M. Dale, and R. Duden. 2000. COP I domains required for coatomer integrity, and novel interactions with ARF and ARF-GAP. *EMBO J.* 19:3905–3917. https://doi.org/10.1093/emboj/19.15.3905

Fresno, C., and E.A. Fernández. 2013. RDAVIDWebService: a versatile R interface to DAVID. *Bioinformatics.* 29:2810–2811. https://doi.org/10.1093/bioinformatics/btt487

Gui, X., H. Yang, T. Li, X. Tan, P. Shi, M. Li, F. Du, and Z.J. Chen. 2019. Autophagy induction via STING trafficking is a primordial function of the cGAS pathway. *Nature.* 567:262–266. https://doi.org/10.1038/s41586-019-1006-9

Haag, S.M., M.F. Gulen, L. Reymond, A. Gibelin, L. Abrami, A. Decout, M. Heymann, F.G. van der Goot, G. Turcatti, R. Behrendt, et al. 2018. Targeting STING with covalent small-molecule inhibitors. *Nature.* 559:269–273. https://doi.org/10.1038/s41586-018-0287-8

Hahn, W.C., S.K. Dessain, M.W. Brooks, J.E. King, B. Elenbaas, D.M. Sabatini, J.A. DeCaprio, and R.A. Weinberg. 2002. Enumeration of the simian virus 40 early region elements necessary for human cell transformation. *Mol. Cell. Biol.* 22:2111–2123. https://doi.org/10.1128/MCB.22.7.2111-2123.2002

Huang, D.W., B.T. Sherman, Q. Tan, J.R. Collins, W.G. Alvord, J. Roayaei, R. Stephens, M.W. Baseler, H.C. Lane, and R.A. Lempicki. 2007. The DAVID Gene Functional Classification Tool: a novel biological module-centric algorithm to functionally analyze large gene lists. *Genome Biol.* 8:R183. https://doi.org/10.1186/gb-2007-8-9-r183

Huttlin, E.L., R.J. Bruckner, J.A. Paulo, J.R. Cannon, L. Ting, K. Baltier, G. Colby, F. Gebreab, M.P. Gygi, H. Parzen, et al. 2017. Architecture of the human interactome defines protein communities and disease networks. *Nature.* 545:505–509. https://doi.org/10.1038/nature22366

Krutzke, S., C. Rietschel, and G. Horneff. 2019. Baricitinib in therapy of COPA syndrome in a 15-year-old girl. *Eur. J. Rheumatol.* 1–4:1–4. https://doi.org/10.5152/eurjrheum.2019.18177

Lee, J.W., X. Fang, N. Gupta, V. Serikov, and M.A. Matthay. 2009. Allogeneic human mesenchymal stem cells for treatment of E. coli endotoxin-induced acute lung injury in the ex vivo perfused human lung. *Proc. Natl. Acad. Sci. USA.* 106:16357–16362. https://doi.org/10.1073/pnas.0907996106

Lee, M.N., M. Roy, S.-E. Ong, P. Mertins, A.-C. Villani, W. Li, F. Dotiwala, J. Sen, J.G. Doench, M.H. Orzalli, et al. 2013. Identification of regulators of the innate immune response to cytosolic DNA and retroviral infection by an integrative approach. *Nat. Immunol.* 14:179–185. https://doi.org/10.1038/ni.2509

Li, S., L. Wang, M. Berman, Y.-Y. Kong, and M.E. Dorf. 2011. Mapping a dynamic innate immunity protein interaction network regulating type I interferon production. *Immunity.* 35:426–440. https://doi.org/10.1016/j.immuni.2011.06.014

Liu, Y., A.A. Jesus, B. Marrero, D. Yang, S.E. Ramsey, G.A.M. Sanchez, K. Tenbrock, H. Wittkowski, O.Y. Jones, H.S. Kuehn, et al. 2014. Activated STING in a vascular and pulmonary syndrome. *N. Engl. J. Med.* 371:507–518. https://doi.org/10.1056/NEJMoa1312625

Liu, S., X. Cai, J. Wu, Q. Cong, X. Chen, T. Li, F. Du, J. Ren, Y.T. Wu, N.V. Grishin, et al. 2015. Phosphorylation of innate immune adaptor proteins MAVS, STING, and TRIF induces IRF3 activation. *Science.* 347. aaa2630. https://doi.org/10.1126/science.aaa2630

Love, M.I., W. Huber, and S. Anders. 2014. Moderated estimation of fold change and dispersion for RNA-seq data with DESeq2. *Genome Biol.* 15:550. https://doi.org/10.1186/s13059-014-0550-8

Manils, J., H. Fischer, J. Climent, E. Casas, C. García-Martínez, J. Bas, S. Sukseree, T. Vavouri, F. Ciruela, J.M. de Anta, et al. 2017. Double deficiency of Trex2 and DNase1L2 nucleases leads to accumulation of DNA in lingual cornifying keratinocytes without activating inflammatory responses. *Sci. Rep.* 7:11902. https://doi.org/10.1038/s41598-017-12308-4

Miller, C.N., I. Proekt, J. von Moltke, K.L. Wells, A.R. Rajpurkar, H. Wang, K. Rattay, I.S. Khan, T.C. Metzger, J.L. Pollack, et al. 2018. Thymic tuft cells promote an IL-4-enriched medulla and shape thymocyte development. *Nature.* 559:627–631. https://doi.org/10.1038/s41586-018-0345-2

Mitrovic, S., H. Ben-Tekaya, E. Koegler, J. Gruenberg, and H.-P. Hauri. 2008. The cargo receptors Surf4, endoplasmic reticulum-Golgi intermediate compartment (ERGIC)-53, and p25 are required to maintain the

architecture of ERGIC and Golgi. *Mol. Biol. Cell*. 19:1976–1990. https://doi.org/10.1091/mbc.e07-10-0989

Mukai, K., H. Konno, T. Akiba, T. Uemura, S. Waguri, T. Kobayashi, G.N. Barber, H. Arai, and T. Taguchi. 2016. Activation of STING requires palmitoylation at the Golgi. *Nat. Commun*. 7:11932. https://doi.org/10.1038/ncomms11932

Mukai, K., E. Ogawa, R. Uematsu, Y. Kuchitsu, T. Uemura, S. Waguri, T. Suzuki, N. Dohmae, H. Arai, A.K. Shum, et al. 2020. Homeostatic regulation of STING by Golgi-to-ER membrane traffic. *bioRxiv*. https://doi.org/10.1101/2020.05.20.107664 (Preprint posted May 21, 2020)

Nedjic, J., M. Aichinger, J. Emmerich, N. Mizushima, and L. Klein. 2008. Autophagy in thymic epithelium shapes the T-cell repertoire and is essential for tolerance. *Nature*. 455:396–400. https://doi.org/10.1038/nature07208

Otero, D.C., D.P. Baker, and M. David. 2013. IRF7-dependent IFN-β production in response to RANKL promotes medullary thymic epithelial cell development. *J. Immunol*. 190:3289–3298. https://doi.org/10.4049/jimmunol.1203086

Ramos, C., M. Montaño, J. García-Alvarez, V. Ruiz, B.D. Uhal, M. Selman, and A. Pardo. 2001. Fibroblasts from idiopathic pulmonary fibrosis and normal lungs differ in growth rate, apoptosis, and tissue inhibitor of metalloproteinases expression. *Am. J. Respir. Cell Mol. Biol*. 24:591–598. https://doi.org/10.1165/ajrcmb.24.5.4333

Shang, J., T. Xia, Q.-Q. Han, X. Zhao, M.-M. Hu, H.-B. Shu, and L. Guo. 2018. Quantitative Proteomics Identified TTC4 as a TBK1 Interactor and a Positive Regulator of SeV-Induced Innate Immunity. *Proteomics*. 18:1700403–1700413. https://doi.org/10.1002/pmic.201700403

Srikanth, S., J.S. Woo, B. Wu, Y.M. El-Sherbiny, J. Leung, K. Chupradit, L. Rice, G.J. Seo, G. Calmettes, C. Ramakrishna, et al. 2019. The Ca^{2+} sensor STIM1 regulates the type I interferon response by retaining the signaling adaptor STING at the endoplasmic reticulum. *Nat. Immunol*. 20:152–162. https://doi.org/10.1038/s41590-018-0287-8

Tsui, J.L., O.A. Estrada, Z. Deng, K.M. Wang, C.S. Law, B.M. Elicker, K.D. Jones, S.D. Dell, G. Gudmundsson, S. Hansdottir, et al. 2018. Analysis of pulmonary features and treatment approaches in the COPA syndrome. *ERJ Open Res*. 4:00017–02018. https://doi.org/10.1183/23120541.00017-2018

Uggenti, C., A. Lepelley, and Y.J. Crow. 2019. Self-Awareness: Nucleic Acid-Driven Inflammation and the Type I Interferonopathies. *Annu. Rev. Immunol*. 37:247–267. https://doi.org/10.1146/annurev-immunol-042718-041257

UniProt Consortium. 2019. UniProt: a worldwide hub of protein knowledge. *Nucleic Acids Res*. 47(D1):D506–D515. https://doi.org/10.1093/nar/gky1049

Volpi, S., J. Tsui, M. Mariani, C. Pastorino, R. Caorsi, O. Sacco, A. Ravelli, A.K. Shum, M. Gattorno, and P. Picco. 2018. Type I interferon pathway activation in COPA syndrome. *Clin. Immunol*. 187:33–36. https://doi.org/10.1016/j.clim.2017.10.001

Watkin, L.B., B. Jessen, W. Wiszniewski, T.J. Vece, M. Jan, Y. Sha, M. Thamsen, R.L.P. Santos-Cortez, K. Lee, T. Gambin, et al; Baylor-Hopkins Center for Mendelian Genomics. 2015. COPA mutations impair ER-Golgi transport and cause hereditary autoimmune-mediated lung disease and arthritis. *Nat. Genet*. 47:654–660. https://doi.org/10.1038/ng.3279

Xing, Y., X. Wang, S.C. Jameson, and K.A. Hogquist. 2016. Late stages of T cell maturation in the thymus involve NF-κB and tonic type I interferon signaling. *Nat. Immunol*. 17:565–573. https://doi.org/10.1038/ni.3419

Supplemental material

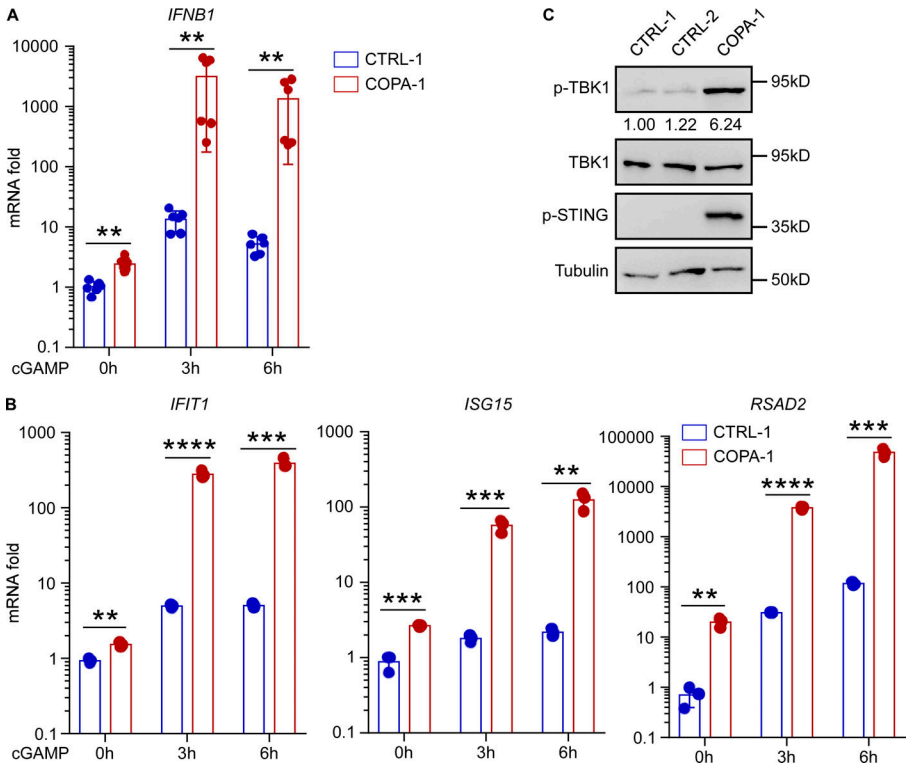

Figure S1. **COPA syndrome patient fibroblasts demonstrate STING activation. (A)** Real-time PCR was performed for *IFNB1* expression in primary lung fibroblasts from a healthy control and a COPA syndrome subject treated with cGAMP (2 µg/ml) for indicated time. Data from six samples in two independent experiments are means ± SD, two-tailed Mann-Whitney *U* test. **(B)** Real-time PCR in triplicate for ISG expression in primary lung fibroblasts from a healthy control and a COPA syndrome subject treated with cGAMP (2 µg/ml) for indicated time. Data are means ± SD, unpaired two-tailed Student's *t* test. **(C)** Immunoblots of primary lung fibroblasts for indicated antibodies. **P < 0.01, ***P < 0.001, ****P < 0.0001.

A

Protein	C terminus	Subcellular location	Function
CCDC47	KQI**K**V**K**AM	ER	Calcium regulation protein
DDOST	MKE**K**E**K**SD	ER	Glycosyltransferase enzyme
HM13	KGLE**KK**EK	ER, Plasma membrane	ER-resident intramembrane protease
MATR3	ERRQ**KK**ET	Nucleus	RNA binding protein
SAC1	LVQ**K**E**K**ID	ER, Golgi	Phosphoinositide phosphatase
STT3B	KKIS**KK**TV	ER	Catalytic subunit of oligosaccharyl transferase
SURF4	**MDEKKKEW**	**ER, ERGIC, Golgi**	**Cargo receptor**

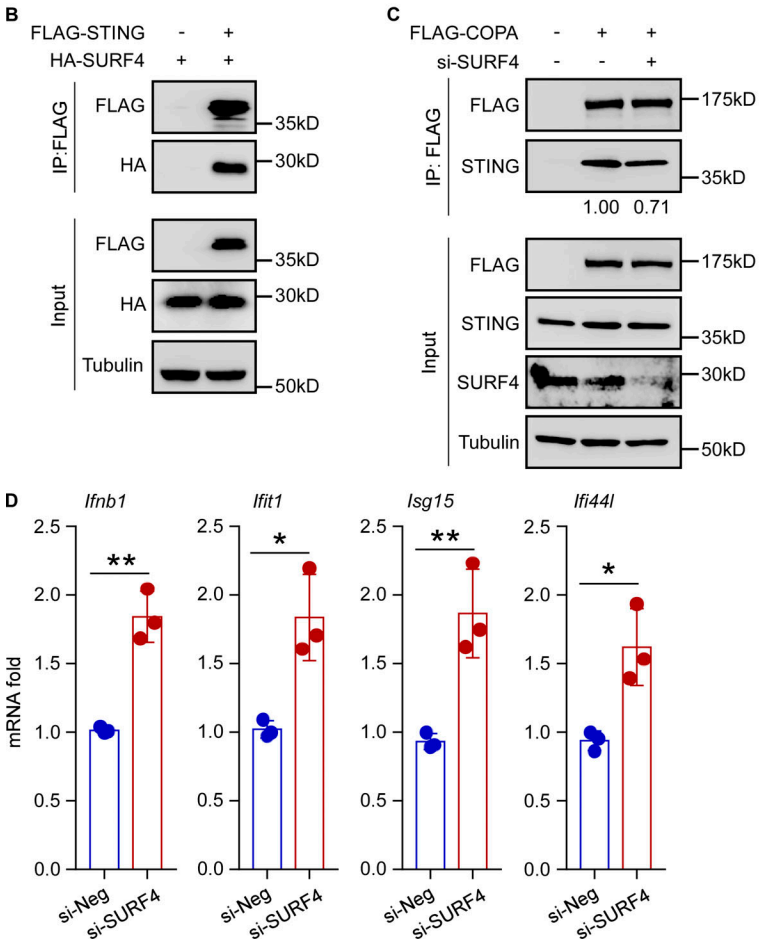

Figure S2. **SURF4 functions as a cargo receptor that mediates retrieval of STING by COPA. (A)** Seven STING interacting partners with C-terminal dilysine motifs were identified in published studies describing STING affinity purification–mass spectrometry data (Lee et al., 2013; Huttlin et al., 2017; Shang et al., 2018; Li et al., 2011; UniProt Consortium, 2019). Shown for each protein are its C terminus sequence with dilysine motif highlighted, subcellular location, and function. **(B)** FLAG IPs from lysates of HEK293T cells overexpressing FLAG-tagged STING and HA-tagged SURF4 were immunoblotted for indicated antibodies. **(C)** HEK293 cells were transfected with FLAG-tagged COPA and si-SURF4 for 48 h. FLAG IPs from lysates of HEK293 cells were immunoblotted for indicated antibodies. **(D)** Real-time PCR in triplicate for ISG expression in immortalized MEF cells with EGFP-STING after si-SURF4 for 48 h. Data represent means ± SD. *P < 0.05, **P < 0.01 (unpaired two-tailed Student's *t* tests). ERGIC, ER-Golgi intermediate compartment; siNeg, nontargeting siRNA control.

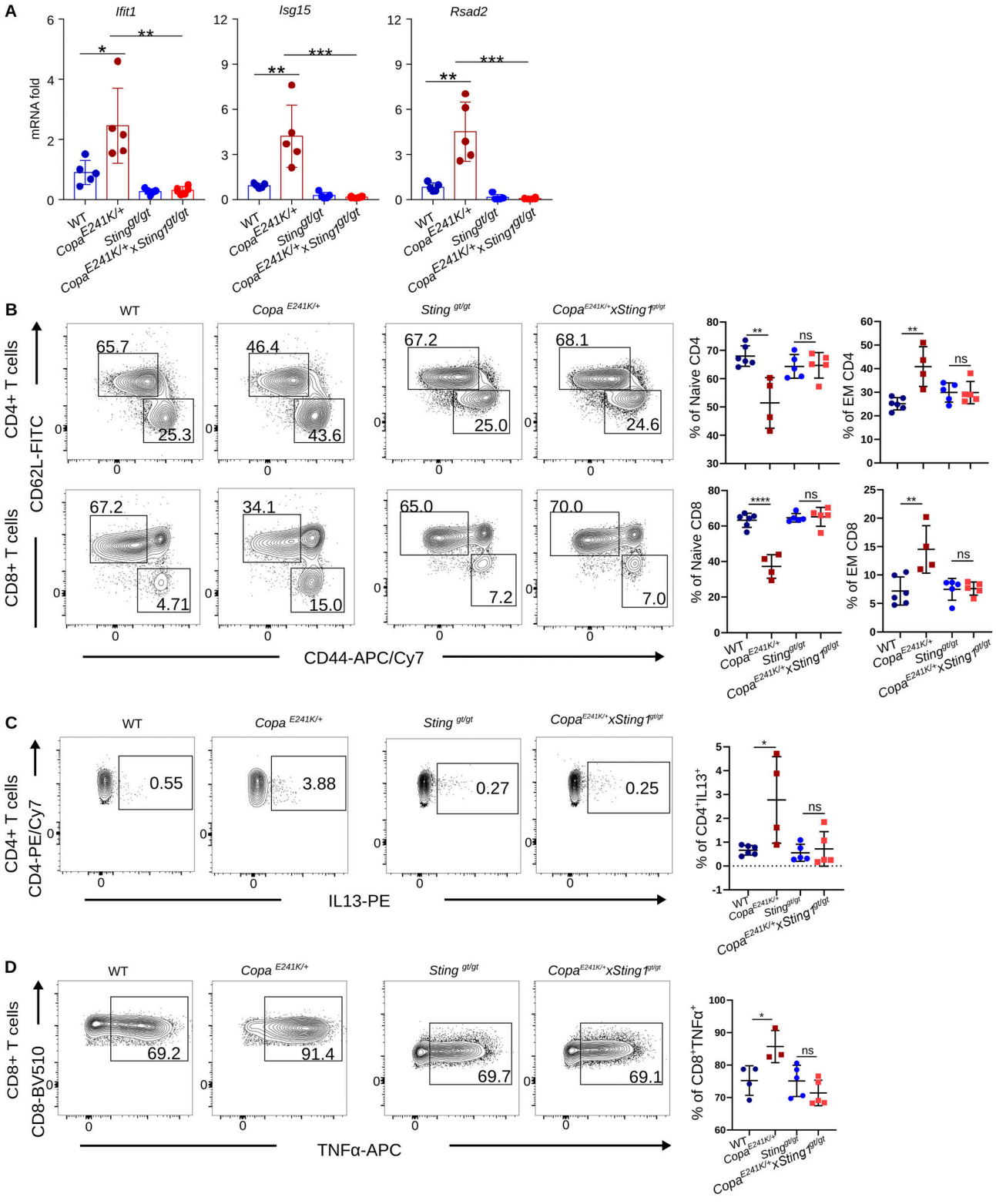

Figure S3. **Activated STING in *Copa*$^{E241K/+}$ mice results in type I interferon–driven inflammation. (A)** Real-time PCR performed for ISG expression in splenocytes from WT (n = 5), *Copa*$^{E241K/+}$ (n = 5), *Sting*$^{gt/gt}$ (n = 5), and *Copa*$^{E241K/+}$×*Sting1*$^{gt/gt}$ (n = 6) mice. **(B)** Left: Representative flow plots showing expression of CD62L versus CD44 on T cells (top: CD4$^+$ T cells; bottom: CD8$^+$ T cells). Right: Percentages of naive and effector memory T cells (left: CD4$^+$ T cells; right: CD8$^+$ T cells). WT: n = 6; *Copa*$^{E241K/+}$: n = 4; *Sting*$^{gt/gt}$: n = 5; *Copa*$^{E241K/+}$×*Sting1*$^{gt/gt}$: n = 5. **(C)** Left: Intracellular levels of IL13 in splenic CD4$^+$ T cells after PMA/ionomycin stimulation. Right: percentages of IL13-producing CD4$^+$ T cells. WT: n = 6; *Copa*$^{E241K/+}$: n = 4; *Sting*$^{gt/gt}$: n = 5; *Copa*$^{E241K/+}$×*Sting1*$^{gt/gt}$: n = 5, more than three independent experiments. **(D)** Left: Intracellular TNF-α production in splenic CD8$^+$ T cells after PMA/ionomycin stimulation. Right: percentages of TNF-α–producing CD8$^+$ T cells. WT: n = 4; *Copa*$^{E241K/+}$: n = 3; *Sting*$^{gt/gt}$: n = 5; *Copa*$^{E241K/+}$×*Sting1*$^{gt/gt}$: n = 5, more than three independent experiments. Data in A–D represent means ± SD. *P < 0.05, **P < 0.01, ***P < 0.001, ****P < 0.0001; ns, not significant (unpaired, parameteric two-tailed Student's t tests).